Polymer Degradation and Stability 229 (2024) 110949

Contents lists available at ScienceDirect

Polymer Degradation and Stability

journal homepage: www.journals.elsevier.com/polymer-degradation-and-stability

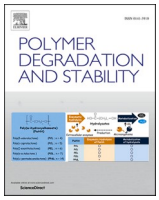

Green synthesis of a P/N/B-containing aggregate for boosting fire-retardancy of PA6/aluminum diethylphosphinate composites

Yixia Lu [a,b,1], Tao Chu [a,1], Siqi Huo [a,d], Guobo Huang [c], Zhiguang Xu [b,*], Jiabing Feng [a,b,*], Hongyan Xie [b], Pooya Jafari [a], Hao Wang [a,e], Pingan Song [a,d,*]

[a] Centre for Future Materials, University of Southern Queensland, Springfield 4300, Australia
[b] College of Biological, Chemical Sciences and Engineering, Jiaxing University, Jiaxing 314001, PR China
[c] School of Pharmaceutical and Chemical Engineering, Taizhou University, Jiaojiang, Zhejiang Province 318000, China
[d] School of Agriculture and Environmental Science, University of Southern Queensland, Springfield, QLD 4300, Australia
[e] School of Engineering, University of Southern Queensland, Springfield, QLD 4300, Australia

ARTICLE INFO

Keywords:
Aluminum diethylphosphinate
Fire retardant
PA6
Synergist

ABSTRACT

The intrinsic flammability of polyamide 6 (PA6) has significantly impeded its broad application regardless of its balanced physical properties. Aluminum diethylphosphinate (ADP), as a P-containing fire retardant, has been demonstrated to be effective in reducing flammability of PA6 because of its dual-phase modes of action by creating an intact protective char layer and inhibiting the burning process. However, the efficiency of ADP needs to be further improved for creating cost-effective fire-retardant PA6, in addition to its relatively high cost. To boost its efficiency, we, here, report a P/N/B-containing aggregate (MBA) as an effective synergist via green self-assembly of melamine (MA), boric acid (BA) and amino trimethylene phosphonic acid (ATMP) in an aqueous medium. The results show that the inclusion of 5 wt% MBA and 10 wt% ADP leads to a significantly reduced peak heat release rate (PHRR) by 52.5% compared to neat PA6, in addition to a desired UL-94 V-0 rating. A synergistic effect of 55.4 % is observed between MBA and ADP in terms of the PHRR value. This work provides a facile green strategy for developing eco-friendly multiple elements-containing fire retardants, which can be used as fire retardants alone or high-efficiency synergists for other fire retardants.

1. Introduction

Because of high mechanical strength, oil resistance, and electrical insulating properties, polyamide 6 (PA6) has been applied in various areas, including electronics and electricity, packaging, and automotive industry [1-4]. Nevertheless, PA6 has been plagued by its non-negligible drawback — intrinsic flammability, as reflected by its low limiting oxygen index (LOI, <22 %) and severe melt-dripping upon burning, thus presenting a grand fire risk and limiting its applications in industries [5-7]. For this reason, it is imperative to develop fire-retardant PA6 to ensure its real-world application.

Incorporating flame-retardant additives has been considered as an efficient and facile strategy to enhance the fire safety of polymers. P- and N-containing compounds have recently emerged as promising alternatives to traditional halogen-based fire retardants which can generate toxic products [8]. P-containing fire retardants (P-FRs) generally can act in both gas and condensed phases during combustion due to the formation of P-derived free radicals and phosphorus/phosphate salts, while N-containing fire retardants (N-FRs) mainly act in gas phase by releasing N-containing inert gases, e.g., NH_3 [9,10]. In comparison, P/N-containing compounds usually possesses a synergistic effect between phosphorus and nitrogen elements [11,12]. In addition, other elements, including sulfur (S) [13], silicon (Si) [14], and boron (B) [15] can strengthen the fire retardancy efficiency by releasing inert gases or by promoting the formation of a more compact char. Typically, boron element is widely applied in the flame-retardant polymers due to its low toxicity, molecular diversity, and carbonization effect. Boron oxides can be formed when B-containing fire retardants (B-FRs) are heated, which can melt to form a glassy char layer above 500 °C to isolate oxygen and prevent heat transfer [16,17]. Besides, B-FRs are well-known for its environmental friendliness and low cost [18-20]. However, boric acid and its derivatives are prone to hydrolyzation, which impedes their

* Corresponding authors.
E-mail addresses: zhiguang.xu@zjxu.edu.cn (Z. Xu), jiabing.feng@zjxu.edu.cn (J. Feng), pingan.song@usq.edu.au, pingansong@gmail.com (P. Song).
[1] Y.X. Lu and T. Chu equally contributed to this work and were listed as co-first authors.

https://doi.org/10.1016/j.polymdegradstab.2024.110949
Received 20 May 2024; Received in revised form 12 July 2024; Accepted 9 August 2024
Available online 12 August 2024

direct use as fire retardants for polymers [21].

Synergistic effects between different fire retardants are proved as a promising way to improve fire-retardant properties as well as to remedy the deficiency of a single fire retardant. Boron-containing additives usually show a synergistic effect with P-FRs or N-FRs [22-24]. For example, besides a superior char-forming ability, melamine borate (MB) not only reduces the burning temperature via its endothermic decomposition, but also dilutes flammable gases via releasing non-flammable products, such as H_2O and NH_3 [25]. The thermal decomposition of melamine can result in the formation of thermally stable substances such as melam, melem, and melon [26,27]. Moreover, boron is found to favor melamine condensation rather than sublimation [28]. For example, 1.5 wt% of a P/N/B-containing hyperbranched oligomer (BDHDP) enabled epoxy resin to achieve reduced heat release and smoke generation during combustion, as reflected by an improved UL-94 rating [29]. However, P/N/B-containing compounds has been rarely developed for fabricating fire-retardant PA6 composites so far.

On the other hand, aluminum diethyl phosphinate (ADP) with high thermal stability has been reported as a highly efficient phosphorous-containing fire retardant for polyamides and other plastics [30]. It acts mainly in gas phase through the release of diethylphosphinic acid. However, apart from its high cost, its contribution to the condensed-phase flame retardancy is relatively weak due to its poor char-forming ability [5,31,32]. To date, several synergists have been developed to improve fire retardancy by either increasing the char residue or decreasing the heat release of PA6/ADP composites, e.g. phosphorus fire retardant diepoxide (DEP) [33], aromatic Schiff base diepoxide (DES) [34], and bismaleimide polyalkyl phosphinate aluminium (BPPA) [35], etc. Nevertheless, the preparation of these synergists often involves the use of organic reagents, which can bring out concerns on human health and the environment.

Given the advantages of boron element, here a P/N/B-containing aggregate (MBA) was synthesized using low-cost melamine (MA), boric acid (BA) and amino trimethylene phosphonic acid (ATMP) in an aqueous solution and used as a synergist for fire-retardant PA6/ADP system. As expected, the introduction of MBA promoted the carbonization of PA6/ADP composites during combustion. Because of the relatively lower cost of MBA than ADP, as-prepared ternary PA6/ADP/MBA shows an advantage than binary PA6/ADP in terms of production costs. The fire-retardant performances were assessed via vertical burning (UL-94), LOI, and cone calorimetry tests, and the mechanical properties were also investigated in detail.

2. Experimental section

2.1. Materials

PA6 (Durethan BC30) was purchased from Lanxess Energizing Chemistry Co., Ltd (German). Melamine (MA), boronic acid (BA), and aluminum diethylphosphinate (ADP) were supplied by Macklin Co., Ltd (China). Amino trimethylene phosphonic acid (ATMP, 95%) was provided by Shandong Taihe Water Treatment Technologies Co., Ltd (China). All chemicals were used directly without further treatment. Ultrapure water (18.2 MΩ) was generated by a Merck Millipore Ultrapurification system.

2.2. Synthesis of MBA

Firstly, to optimize the molar ratio for synthesizing MBA, a pre-experiment was conducted by employing various molar ratios (MA:BA:ATMP = 2:1:1; 2:1:2; 2:2:1; 3:1:1; 3:1:2; and 3:2:1) of MA, BA, and ATMP to produce a series of MBA products. These products were characterized by scanning electron microscopy (SEM), X-ray diffraction (XRD), and X-ray photoelectron spectroscopy (XPS) to explore their morphology, crystallinity, binding modes, and elemental composition. All as-prepared MBA compounds possess almost the same chemical compositions, including B_{1s} (~20.7 at%), C_{1s} (~27.6 at%), N_{1s} (~25.5at %), O_{1s} (~20.0 at%), and P_{2p} (6.6 at%), as demonstrated in Table S1. Three kinds of MBA products with molar ratio of 3:2:1, 3:1:2 and 2:2:1are further investigated by SEM and XRD. All of them possess micro-scale flakes appearance (Fig. S1a) and similar XRD diffraction with the peaks at 12.5 °, 18.8 °, 25.1 °, 27.1 ° (Fig. S1b). The results showed few differences among these MBA compounds, indicating that the chemical structure/composition of the final MBA product is independent on the feeding ratios of raw materials.

Moreover, all these MBA products display similar thermal degradation behaviors, as shown in thermogravimetric analysis (TGA) curves in Fig. S1c. The molar ratio of 3:1:2 was chosen as the most suitable one regarding its highest yield (~70 %). Typically, 18.9 g of MA was thoroughly dissolved in 600 mL ultrapure water at 90 °C in a round flask, and 3.1 g of BA and 31. 5 g of ATMP were dissolved in 100 mL ultrapure water. The obtained BA-ATMP solution was then added dropwise into the MA solution *via* a pressure-equalizing dropping funnel under magnetic stirring and stirred at 90 °C for 2 h. The white solid powder was generated progressively. Finally, the MBA powder was obtained after filtration, washing and vacuum-drying at 100 °C overnight.

2.3. Preparation of PA6/MBA/ADP (FRPA6) composites

PA6 pellets were dried at 80 °C for at least 4 h before use. FRPA6 containing MBA and ADP with a total flame retardant addition of 15 wt % are denoted as MBA_{15}, MBA_6/ADP_9, MPA_5/ADP_{10}, and ADP_{15}, where the number in the subscript represents the loading level of fire retardants. The dried pellets were melt-blended with or without flame retardants at 220 °C for 6 min with a rotor speed of 60 r/min in a HAPRO torque rheometer (RM-200C). Then, the resultant PA6 and FRPA6 products were molded into desired shapes via hot-pressing at 230 °C under 10 MPa for 2 min, followed by a quick cool-press.

2.4. Characterizations

Fourier transform infrared (FT-IR) spectra were recorded by a FT-IR spectrometer (Thermofisher IS50). XPS was performed on a Thermo Scientific K-Alpha equipment with Al Kα radiation ($h\nu$=1486.6 eV). XRD was conducted with Cu Kα radiation (λ=0.1542 nm) on an X-ray diffractometer (XRD-7000, Shimadzu). SEM and energy dispersive spectroscopy (EDS) were presented on a Helios5CX (Thermo Fisher Scientific). Transmission electron microscope (TEM) and EDS mapping were conducted on a Talos F200X (Thermo Fisher Scientific). TGA was performed on a thermogravimetric analyzer (DSC3+/TRACE 1300-ISQ7000, Thermo Fisher Scientific) from 25 °C to 1000 °C with a heating rate of 10 °C/min, under nitrogen and air atmosphere, respectively.

2.5. Measurements

Vertical burning test (UL-94) was conducted on a CZF-2 instrument (Jiangning), with the specimen size of 130 mm × 13 mm × 3.2 mm. Limiting oxygen index (LOI) values were obtained by a JF-3 type oxygen index meter (sample dimensions: 80 mm × 10 mm × 4 mm) in accordance with ASTM D2863–2009. Cone calorimetry test was carried out on a calorimeter (FTT, UK) with a heat flux of 50 kW/m^2 in accordance with ISO 5660, with the specimen dimension of 100 mm × 100 mm × 3.0 mm. Thermogravimetric-infrared spectrometry (TG-IR) was performed on a thermogravimetric analyzer (TGA8000, PerkinElmer) linked to a FT-IR spectrometer (Spectrum 3, PerkinElmer) under N_2 atmosphere at a ramp up of 20 °C/min from 50 to 800 °C. Mechanical properties were explored via an electronic universal testing machine (UTM2503, Sans) with a crosshead rate of 5.0 mm/min based on GB/T 1040.

2.6 Fire safety assessment

To evaluate the fire safety of PA6 and FRPA6, fire growth index (*FGI*)

and fire performance (*FPI*), are used to evaluate the fire performance with equations (1) and (2) [36,37], implying the fire propagation and flashover inclination, respectively. The low value of FGI and high value of FPI indicate the slow fire propagation and low flashover possibility.

$$FGI = PHRR/t_{PHRR} \tag{1}$$

where t_{PHRR} refers to time to reach PHRR.

$$FPI = TTI/PHRR \tag{2}$$

Meanwhile, the fire retardancy index (*FRI*) is defined as the ratio of $THR \times (PHRR/TTI)$ of the neat PA6 to that of FRPA6 as shown in Eq. (3) [38,39], where THR, PHRR, TTI mean total heat release, peak heat release rate and time to ignition, respectively. The value indicates the tendency of the fire retardancy of polymer, specifically, the values <1, 1~10, >10 are taken as "Poor", "Good", "Excellent" performance, respectively.

$$FRI = [THR \times (PHRR/TTI)]_{PA6}/[THR \times (PHRR/TTI)]_{FRPA6} \tag{3}$$

The term synergistic effect (*SE*) is a typical tool for characterization of the synergistic system. It is defined as the ratio of the fire-retardant efficiency of the additive plus the synergist to that of the additive alone. The fire-retardant efficiency involves various parameters, including LOI, char yields, heat release reduction, etc. [40]. Herein, the following Eqs. (4) and (5) are used to evaluate the synergistic effect between MBA and ADP in PA6 [41].

$$P_{Calculated} = P_{MBA} \times \phi_{MBA} + P_{ADP} \times \phi_{ADP} \tag{4}$$

$$SE = \left(P_{Calculated} - P_{Experimental}\right)/P_{Calculated} \tag{5}$$

where *SE* refers to the synergistic effect, *P* refers to the value of PHRR, THR, and AEHC, ϕ refers to the ratio of MBA or ADP in FRPA6, respectively [37].

The quantitative assessment of the fire-retardant mechanism is investigated regarding the flame inhibition (gas phase), charring effect and barrier-protective effect (condensed phase) based on the theory and Eqs. (6-9) from literatures [36,42,43].

$$Flame\ inhibition = THE/TML \tag{6}$$

or

$$Flame\ inhibition = 1 - AEHC_{FRPA6}/AEHC_{PA6} \tag{7}$$

$$Charring\ effect = (Residue_{FRPA6} - Residue_{PA6})/(1 - Residue_{PA6}) \tag{8}$$

$$Barrier - protective\ effect = 1 - (PHRR_{FRPA6}\ /\ PHRR_{PA6})/(THR_{FRPA6}\ /\ THR_{PA6}) \tag{9}$$

Where *THE* is the total heat evolved, also deemed as the *THR* at the time to flame-out, *TML* is the total mass loss, *AEHC* is the average effective heat of combustion, respectively.

3. Results and discussion

3.1. Characterization of MBA

The green synthesis route of MBA is illustrated in Fig. 1a, where a supramolecular aggregate (MBA) is formed by reacting MA, BA and ATMP in an aqueous medium. The SEM (Fig. 1b), TEM images, and EDS mappings (Fig. 1c and d) confirm that MBA possesses a micro-sized plate structure and contains B, C, N, O, and P elements.

As shown in Fig. 2a, for MA, the characteristic absorption peaks at 3470, 3417, 3334 and 3127 cm^{-1} in its FTIR spectrum belong to the stretch vibration of $-NH_2$ groups, and those at 1652, 1553 and 1026 cm^{-1} are ascribed to $N-H$ bending vibration, C = N vibration, and C – N vibration, respectively. For ATMP, the characteristic peaks at 1145 and 933 cm^{-1} are attributed to the vibration of $P = O$ and $P-OH$, respectively [5]. For BA, the absorption peaks at 3201 and 1193 cm^{-1} are assigned to the stretch vibration of $B-OH$, while that at 1459 cm^{-1} is

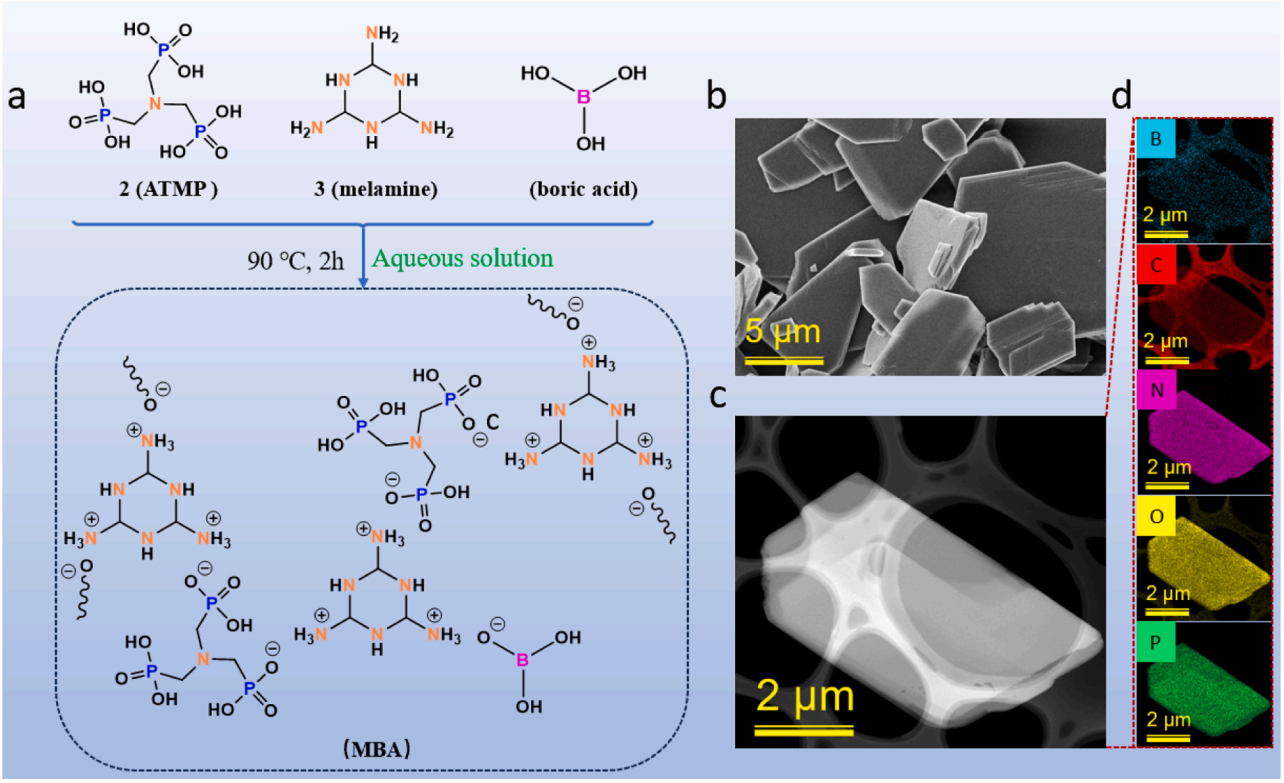

Fig. 1. Synthesis and characterization of MBA: (a) Schematic illustration, (b) SEM image, (c) TEM image, and (d) EDS mapping of MBA.

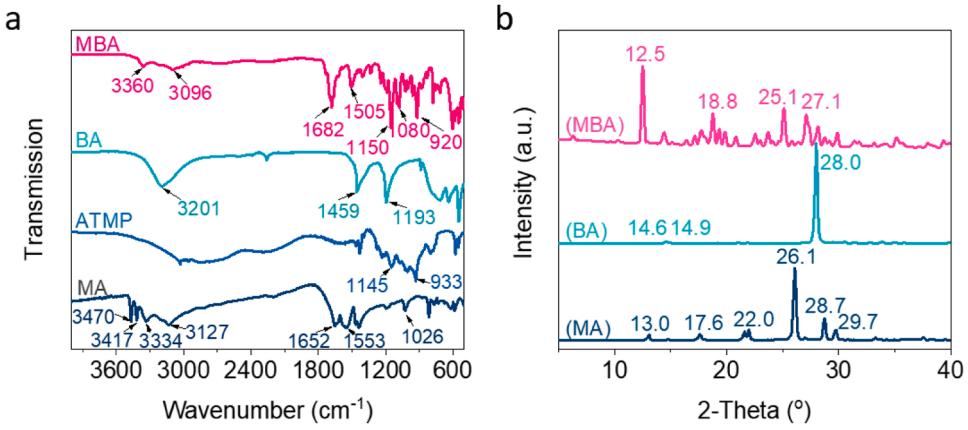

Fig. 2. (a) FTIR spectra and (b) XRD patterns of MA, ATMP, BA, MBA.

attributed to $B-O$ [24,44]. For MBA, there are weak peaks at 3360 and 3096 cm^{-1}, which belong to the vibrations of $-NH_2$ from triazine ring after complexation reaction. The peaks of $N-H$, C = N and C − N shift to 1682, 1505, and 1080 cm^{-1}, further confirming the complexation reaction between MA, ATMP and BA. There are two sharp peaks at 1150 and 920 cm^{-1}, which are presumably assigned to the vibration of $O-B-O/P=O$ and P–OH derived from BA and ATMP, respectively. Noticeably, the peak at 1682 cm^{-1} is assigned to the vibration of NH_3^+. These results imply the successful synthesis of MBA.

Fig. 2b presents the XRD patterns of MA, BA, and MBA. The crystalline structure of MA is clearly confirmed by the peaks at 13.0° (−101), 17.6° (−111), 22.0° (210), 26.1° (−301), 28.7° (−311) and 29.7° (310), which are in compliance with the standard JCPDS card No 24–1654 [45]. BA features a typical crystalline structure with a sharp peak at 28° (002) and two weak peaks at 14.6° (010) and 14.9° (100). In comparison, multiple peaks can be observed for MBA, indicating that it contains different crystalline structures. Notably, the diffraction peaks at 12.5°, 18.8°, 25.1°, and 27.1° reveal the successful formation of MBA.

The elemental composition of MBA was determined by XPS, as shown in Fig. 3a. One can see the binding energy (BE) peaks of boron (B_{1s}, 190.1 eV, 20.6 at%), carbon (C_{1s}, 288.2 eV, 27.3 at%), nitrogen (N_{1s}, 399.0 eV, 25.5 at%), oxygen (O_{1s}, 531.7 eV, 20.0 at%), and phosphorus (P_{2p}, 133.1 eV, 6.6 at%). Clearly, boron element is present in the newly synthesized MBA in the form of $B-O$ group, as shown in the XPS high resolution spectrum of B element (Fig. 3b). The high resolution O_{1s} spectrum (Fig. 3c) can be divided into the peaks at 532.8 eV ($O-B$), 531.6 eV ($O=P$), 530.3 eV ($O-H$) and 529.6 eV($O-P$), indicative of the existence of oxygen-containing groups.

The thermal properties of MBA were investigated by TGA in both air and nitrogen atmospheres (Fig. 4a and Table 1). The T_5 (the temperature where 5 wt% mass loss occurs) value of MBA is about 292 °C (under air and N_2 atmosphere). Additionally, its temperature at maximum weight loss rate (T_{max}) is 358 °C (air) / 371 °C (N_2), with the mass loss rate (R_{ml}) of 0.35 wt%/ °C in both air and N_2 atmosphere. MBA leaves many residues after heating to 800 °C (35.5 wt% in air and 46.6 wt% in N_2). Clearly, MBA shows satisfied thermal stability that can meet the melt processing of PA6 and has a high charring ability at high temperatures.

3.2. Thermal stability of PA6 and FRPA6

As presented in Fig. 4 and Table 1, PA6 shows a T_5 value of 393 °C and a T_{max} value of 462 °C, with a R_{ml} of 2.0 wt%/ °C, and a poor charring ability (0.5 wt% at 800 °C). Upon the addition of 15 wt% MBA, the T_5 value of MBA_{15} reduces to 290 °C, whilst its R_{ml} decreases to 1.3 wt%/ °C and char residue increases to 11.2 wt%. In comparison, 15 wt% of ADP enables PA6 to retain its onset decomposition temperature (T_5), with slightly declined T_{max} and R_{ml}, and an increased residue of 6.1 wt% at 800 °C. Surprisingly, the combination use of MBA and ADP enables PA6 to maintain its thermal stability and to improve its charring ability, as evidenced by the increased T_{max} (~ 450 °C), decreased R_{ml} (1.4 ~ 1.6 wt% / °C), and increased char residues (7.4 ~ 7.6 wt%) relative to ADP_{15}. Moreover, by comparing the theoretical residue (the sum of the individual contributions) to the experimental data of the FRPA6, the latter gives higher values, specifically, MBA_6/ADP_9 and MBA_5/ADP_{10} leave 6.6 wt% (experimentally) and 2.8 wt%/3.0 wt% (theoretically) of residues at 1000 °C, respectively, while ADP_{15} gives 6.1 wt% and 3.5 wt % correspondingly. The results indicate an enhanced high-temperature stability and a charring ability of ternary PA6/ADP/MBA composites relative to binary ADP_{15}.

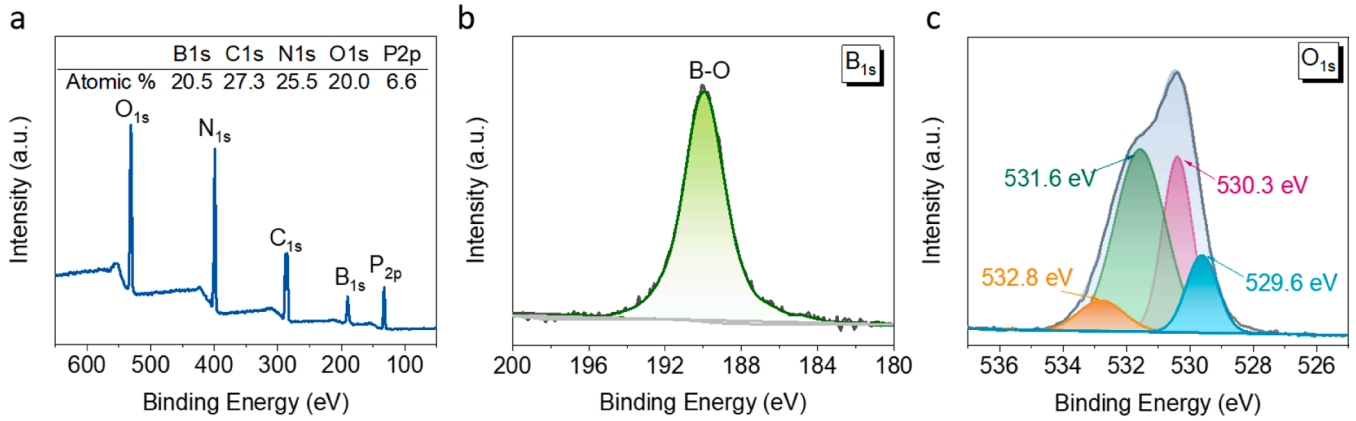

Fig. 3. (a) Full-scan XPS spectrum of MBA and high-resolution spectra of (b) B_{1s} and (c) O_{1s}.

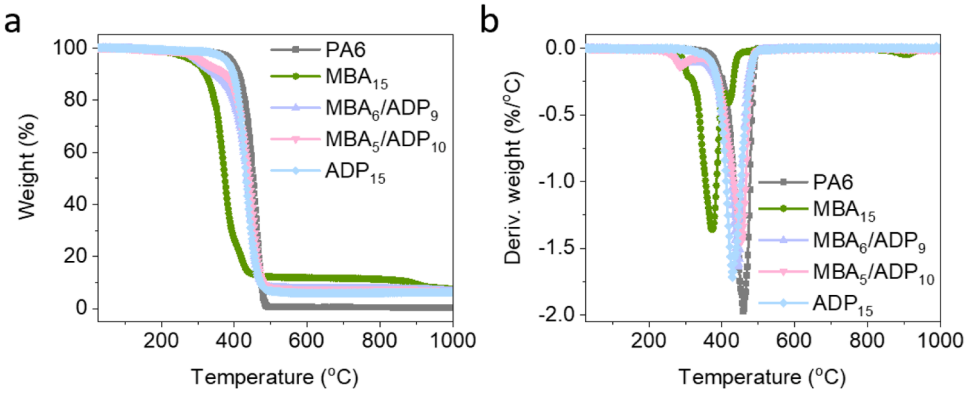

Fig. 4. TG (a) and DTG (b) curves of PA6 and FRPA6 in N_2 atmosphere.

Table 1
TGA results of MBA, ADP, PA6 and FRPA6 under nitrogen atmosphere.

Sample	T_5 [a] (°C)	T_{max} [a] (°C)	R_{ml} [b] (wt% / °C)	Residue at 800 °C (wt%)		Residue at 1000 °C (wt%)	
				Experimental	Theoretical	Experimental	Theoretical
MBA	292 (air, N_2)	358 (air)/ 371 (N_2)	0.35 (air, N_2)	35.5 (air)/46.6 (N_2)	-	22.5 (air)/ 10.0 (N_2)	–
ADP	419	481	1.9	21.8	–	21.2	–
PA6	393	462	2.0	0.5	–	0.4	–
MBA_{15}	290	375	1.3	11.2	7.4	7.5	1.8
MBA_6/ADP_9	300	445	1.6	7.6	5.2	6.6	2.8
MBA_5/ADP_{10}	309	454	1.4	7.4	4.9	6.6	3.0
ADP_{15}	380	429	1.7	6.3	3.7	6.1	3.5

[c] *Theoretical* values refer to the sum of the individual contributions to residues.
[a] T_5 and T_{max} refer to the temperature where 5 % mass loss and the maximum weight loss rate occur, respectively;.
[b] R_{ml} refers to the mass loss rate;.

3.3. Fire retardancy of FRPA6

The fire retardancy of PA6 and its composites were assessed by UL-94 vertical burning, LOI, and cone calorimetry tests, with the results presented in Fig. 5 and Table 2. PA6 is highly flammable, as reflected by its low LOI of 23.2 % and a UL-94 V-2 rating. The addition of 15 wt% MBA reduces the LOI value to 22.3 % and does not contribute to the UL-94 rating, revealing its limited fire-retardant efficiency. In comparison, the incorporation of 15 wt% ADP imparts satisfactory fire retardancy to PA6 with an UL-94 V-0 classification and a high LOI value (32.2 %). By contrast, the introduction MBA and ADP also endows PA6 with satisfactory fire retardancy (Fig. 5a). For instance, the LOI and UL-94 classification of MBA_5/ADP_{10} can reach 26.8 % and V-0, respectively.

Cone calorimetry testing, as one of bench-sale fire tests, has been extensively used to evaluate the combustion behaviors of polymers [46]. As shown in Fig. 5b-e and Table 3, neat PA6 exhibits a high PHRR (522.1 kW/m^2), THR (106.5 MJ/m^2), AEHC (29.7 MJ/Kg), maximum average heat release rate (MARHE, 275.4 kW/m^2) and a low residue (3.7 wt%), revealing its high flammability and poor charring ability. Upon the addition of 15 wt% MBA, the PHRR and MARHE values increase to 849.0 kW/m^2 and 405.4 kW/m^2, respectively, despite a much higher residue of 11.4 wt%, reflecting its significantly improved charring ability but an unsatisfactory effect in reducing heat release. On the contrary, the introduction of 15 wt% ADP into the PA6 matrix brings about decreased PHRR (410.1 kW/m^2, by 21.5 %), THR (96.3 MJ/m^2, by 9.6 %), AEHC (25.3 MJ/Kg, by 10.5 %), and almost unchanged MARHE value, accompanied by an increased residue (7.5 wt%), implying an improved fire safety. In comparison, the combination of MBA and ADP improves the fire retardancy of PA6 to a larger extent. For example, the PHRR value declines to 318.2 kW/m^2 (by 39.1 %) for MBA_6/ADP_9, and to 248.1 kW/m^2 (by 52.5 %) for MBA_5/ADP_{10}. The same trend is also found in THR, AEHC and MARHE values, which indicates significant heat inhibition and thus superior fire retardancy for PA6.

As shown in Fig. 5b, the shapes of curves reflect the heat release rate tendency as the burning proceeds. Specifically, the addition of 15 % of MBA leads to a sharp PHRR peak, indicating its poor heat release inhibition effect. Meanwhile, the early start of heat release of the FRPA6 is ascribed to the early decomposition of MBA and the catalysis of ADP [30]. The plateau of the curves implies the formation of a thermally stable char layer [36], among which MBA/ADP-based samples generate more residues than ADP_{15}. As a result, the heat release slows down to a large extent and the burning time is extended. Additionally, two PA6/MBA/ADP composites generate abundant residues (10.7 wt% and 8.9 wt%), conducing to the isolation of heat and air during burning. In comparison, MBA_{15} leaves a high char residue (11.4 wt%) with a char height of 3 cm (Fig. 5g), while MBA_5/ADP_{10} (Fig. 5h) leaves a more char residue than ADP_{15} (Fig. 5i).

FGI, FPI, and FRI are further calculated to evaluate the fire performance of as-prepared FRPA6. As shown in Table 3, MBA_6/ADP_9 gives rise to the lowest FGI value of 1.22 m^2·s/kW, indicating the lowest possibility of fire propagation among all composites. On the other hand, MBA_5/ADP_{10} brings about the highest FPI of 0.31 kW/m^2·s, implying the best fire safety compared to virgin PA6. This is also evidenced by the highest FRI of 1.84, strongly indicating its “good” fire retardancy as the index value is over 1.0 [38,39]. These results further imply that the combination of MBA and ADP can provide better fire protection for the underlying PA6 matrix.

Consequently, it is reasonable to conclude that there is a synergy existing between MBA and ADP in improving the fire safety of PA6. The term synergistic effect (SE) is a typical tool for characterization of a synergistic system. It is defined as the ratio of the FR efficiency of the additive plus the synergist to that of the additive alone [40]. The FR effectivity involves various parameters, including LOI, char formation, heat release, etc. Herein, Eqs. (4 and 5) are used to evaluate the SE, as demonstrated in Section 2.6. As exhibited in Fig. 6a and Table S2, the

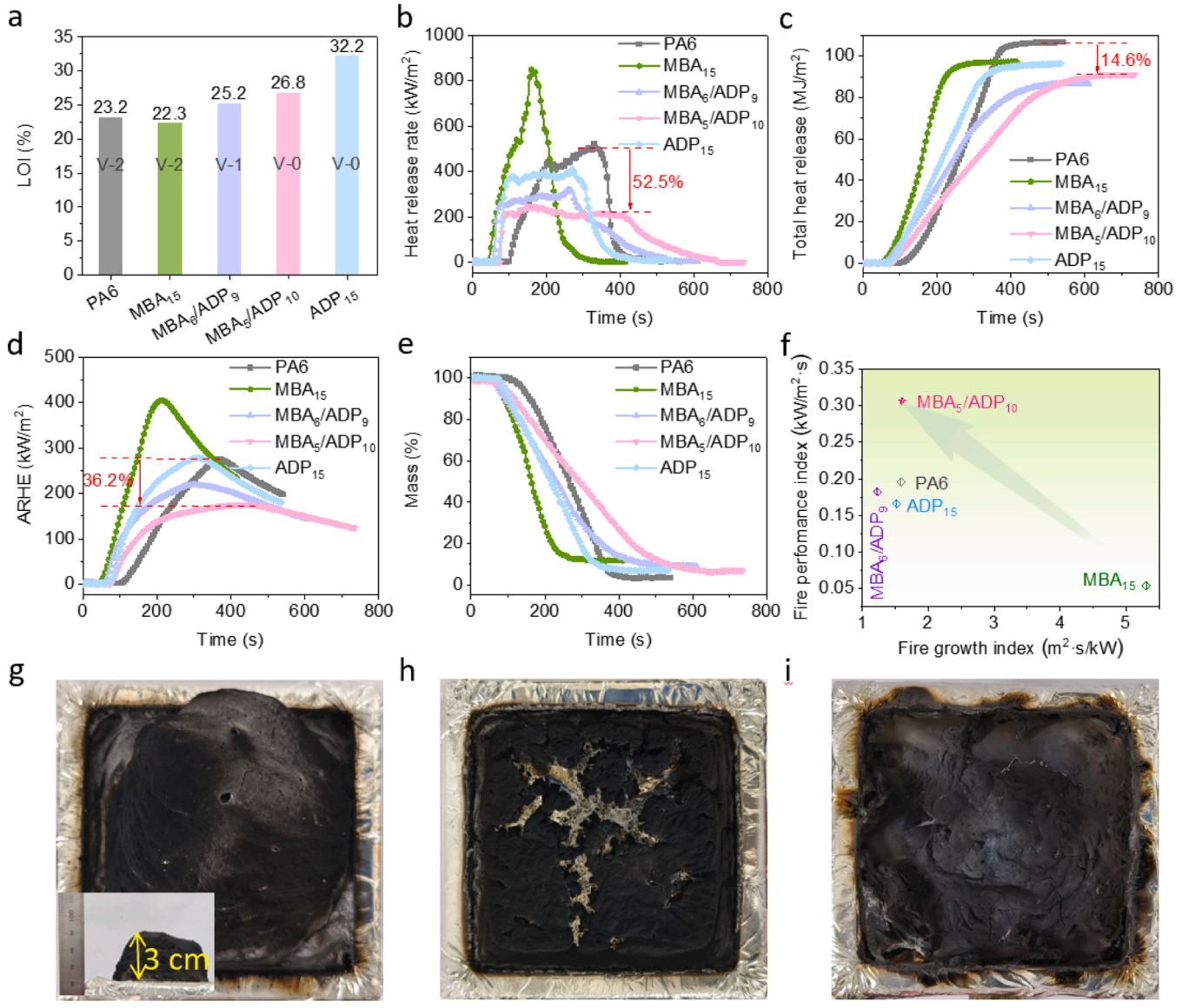

Fig. 5. (a) LOI values and UL-94 ratings, (b) HRR curves, (c) THR curves, (d) ARHE curves, (e) mass loss curves, (f) scatter plot of fire performance index versus fire growth index, and digital photos of (g) MBA_{15}, (h) MBA_5/ADP_{10}, and (i) ADP_{15} chars.

Table 2
Vertical burning ratings and LOI values of PA6 and FRPA6.

Sample	UL-94			
	t_1/t_2 [a](s)	Dripping/Cotton ignition	Rating	LOI (%)
PA6	19/7	Yes/Yes	V-2	23.2
MBA_{15}	20/18	Yes/Yes	V-2	22.3
MBA_6/ADP_9	13/11	No/No	V-1	25.2
MBA_5/ADP_{10}	9/6	No/No	V-0	26.8
ADP_{15}	8/5	No/No	V-0	32.2

[a] t_1 and t_2 refer to the burning times after the first and second ignition, respectively.

combination use of MBA and ADP devotes marginal synergistic effect in terms of THR and EHC (5.7 ~ 10.2 %) relative to those calculated from the individual contributions in fire assessment. However, both MBA_6/ADP_9 and MBA_5/ADP_{10} show an evident synergy in terms of PHRR reduction (45.7 %, 55.4 %). The proportion control of additives is vital (resulting in 10 % synergy promotion) even if there is an only 1 % deviation.

3.4. Fire-retardant mechanism

The fire-retardant mechanism regarding the gas phase and condensed phase was explored, such as the flame inhibition acts in gas phase, while the charring effect and barrier-protective effect act in condensed phase. The three effects can be quantitatively calculated according to the Eqs. (6)-(9), with results listed in Table S2 and Fig. 6b. The total heat released at the time to flame-out per released volatiles, which can be regarded as the reduction in the effective heat of combustion of the volatiles (*THE/TML*), acts as the main flame inhibition effect [42,47]. The quotient value of *THE/TML* (Eq. (6)) is inversely proportional to the effect of the flame inhibition. For example, MBA_5/ADP_{10} possess the lowest *THE/TML* value (2.8 MJ/m^2g), and thus the best flame inhibition. This phenomenon is attributed to the high reactivity of phosphorus free radicals degraded from MBA and ADP. This result can also be verified by its higher CO yield (0.09 $kg\ kg^{-1}$) than pure PA6, implying the incomplete combustion of the sample MBA_5/ADP_{10} resulted from the flame inhibition effect. As AEHC is deemed as the average heat release by unit mass loss and can be calculated as the mean ratio of HRR to mass loss rate in a certain burning time, another simple

Table 3
Cone calorimetry testing results and fire performances of PA6 and FRPA6.

Sample	TTI [a] (s)	PHRR [b] (kW/m^2) (Δ%)	THR [c] (MJ/m^2) (Δ%)	AEHC [d] (MJ/Kg) (Δ%)	MARHE [e] (kW/m^2) (Δ%)	Residue (wt%)	Mean COY [f] (kg kg^{-1})	Mean CO_2Y [f] (kg kg^{-1})	FGI [g] (m^2·s/kW)	FPI [h] (kW/m^2·s)	FRI (category) [i]
PA6	102	522.1	106.5	29.7	275.4	3.7	0.02	1.87	1.58	0.20	–
MBA_{15}	46	849.0 (↑62.6 %)	97.0 (↓8.9 %)	26.0 (↓3.3 %)	405.4 (↑47.2 %)	11.4	0.02	1.82	5.31	0.05	0.30 (Poor)
MBA_6/ADP_9	58	318.2 (↓39.1 %)	86.7 (↓18.6 %)	24.3 (↓14.4 %)	218.1 (↓20.8 %)	10.7	0.09	1.44	1.22	0.18	1.15 (Good)
MBA_5/ADP_{10}	76	248.1(↓52.5 %)	91.0 (↓14.6 %)	25.0 (↓15.3 %)	175.8 (↓36.2 %)	8.9	0.09	1.44	1.60	0.31	1.84 (Good)
ADP_{15}	68	410.1 (↓21.5 %)	96.3 (↓9.6 %)	25.3 (↓10.5 %)	277.8 (↑0.9 %)	7.5	0.09	1.52	1.52	0.17	0.94 (Poor)

[a] TTI: Time to ignition;.
[b] PHRR: Peak heat rate release;.
[c] THR: Total heat release;.
[d] AEHC: Average effective heat of combustion;.
[e] MARHE: Maximum average heat release rate;.
[f] Mean COY and Mean CO_2Y: mean CO and CO_2 yields.
[g] FGI: Fire growth index;.
[h] FPI: Fire performance index;.
[i] FRI (category): Fire retardant index and the category of fire retardancy.

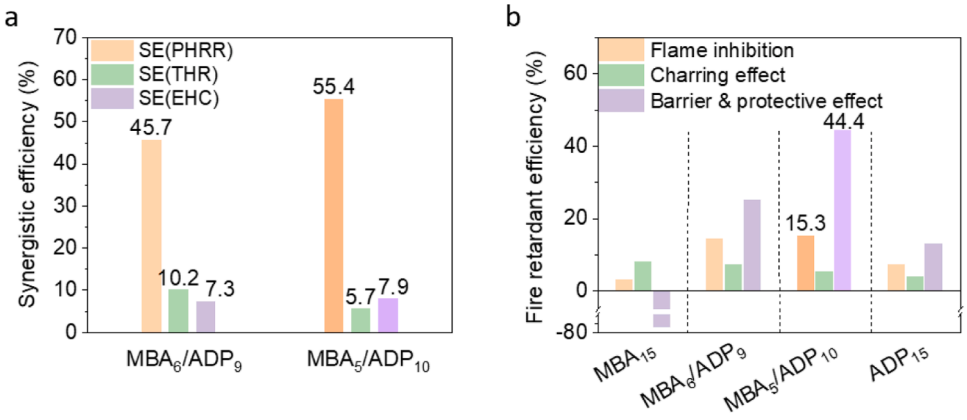

Fig. 6. (a) Synergistic effect of MBA_6/ADP_9 and MBA_5/ADP_{10}, and (b) quantitative assessment of fire-retardant mode of FRPA6 samples.

method to evaluate the flame inhibition is developed by calculating the AEHC reduction ratio [$1-AEHC_{FRPA6}/AEHC_{PA6}$] in Eq. (7) [43]. The ratios are proportional to the flame inhibition effect, among which MBA_5/ADP_{10} manifests superior (15.3 %) to the other samples.

Similarly, the charring effect is investigated by the difference percentage of the total mass loss ratio between FRPA6 and PA6 [($Residue_{FRPA6}$–$Residue_{PA6}$)/(1–$Residue_{PA6}$)], as shown in Eq. (8) [43]. The highest value of 8.1 % for sample MBA_{15} indicates its good charring ability, yet poor fire retardancy attributed to its incompact char layers, as demonstrated in the SEM images (Fig. 7). Nevertheless, as the amount of ADP increases, the charring effect weakens (from 7.3 % for MBA_6/ADP_9 to 4.0 % for ADP_{15}), confirming the insufficient charring ability of ADP. The introduction of MBA into PA6/ADP composites can enhance the charring ability (by 35 % to 82.5 %), confirming a synergistic effect between MBA and ADP. The char residue, as a barrier for heat and fuel transfer, affects the heat release. Thus, the barrier-protective effect can be evaluated by using the relatively hindered heat release [1-($PHRR_{FRPA6}$/$PHRR_{PA6}$)/(THR_{FRPA6}/THR_{PA6})] in Eq. (9). As a result, the sample MBA_5/ADP_{10} shows the best barrier-protective effect with the value of 44.4 %, followed by the sample MBA_6/ADP_9 (25.1 %). ADP_{15} manifests a poor barrier-protective effect mainly because of its small amount of residue. The minus value (−78.5 %) of MBA_{15} elucidates a negative barrier-protective effect as its char is slightly intumescent but porous and incompact, and thus cannot act as an effective thermal barrier for heat exchange (see digital photo and SEM image in Fig. 5g, Fig. 7$a_{3–4}$). Above results and discussion clearly indicate that the MBA/ADP combination plays a key role in both gas and condensed phases.

To further investigate the fire-retardant mechanism, Raman spectroscopy, XPS analysis, and SEM imaging of chars and TG-IR spectroscopy were conducted, as depicted in Fig. 7. Clearly, all Raman spectra of the char residue present D peak (at ~1380 cm^{-1}) and G peak (at ~1600 cm^{-1}) (Fig. 7a_1-c_1). The char of MBA_5/ADP_{10} gives the lowest area ratio of D band to G band (A_D/A_G) (2.6) compared to the chars of MBA_{15} and ADP_{15} (3.5 and 3.0), indicating the highest graphitization degree [48]. Both chars of MBA_{15} and MBA_5/ADP_{10} contain boron element (B_{1s}, 190.9/191.6 eV) besides carbon (C_{1s}, 284.0 eV), oxygen (O_{1s}, 531.9 eV), nitrogen (N_{1s}, 400.0 eV), and phosphorus (P_{2p}, 133.5 eV and P_{2s}, 191 eV) elements, whilst the char of MBA_5/ADP_{10} includes aluminum (Al_{2s}, 119.0 eV; Al_{2p}, 74.9 eV) element. Besides, aluminum can also be found in the char residue of ADP_{15} (Fig. 7a_2-c_2).

The SEM images of the external chars (Fig. 7a_3-c_3) and the internal chars (Fig. 7a_4-c_4) show that MBA_{15} only leaves a porous and incompact char after combustion, while the char of MBA_5/ADP_{10} is dense both internally and externally. However, ADP_{15} leaves a compact external char layer with a tunnel-like internal structure after burning. Therefore, the P/N/B-containing MBA imparts enhanced fire retardancy to PA6/ADP composite by its condensed-phase effect. TG-IR spectra (Fig. 7d) depict the released fragment in gas phase at 450 °C. The sharper peaks at 2940 cm^{-1} (C – H), 1710 cm^{-1} (C = O) and 1150 cm^{-1} (*P* = *O*) of ADP_{15}

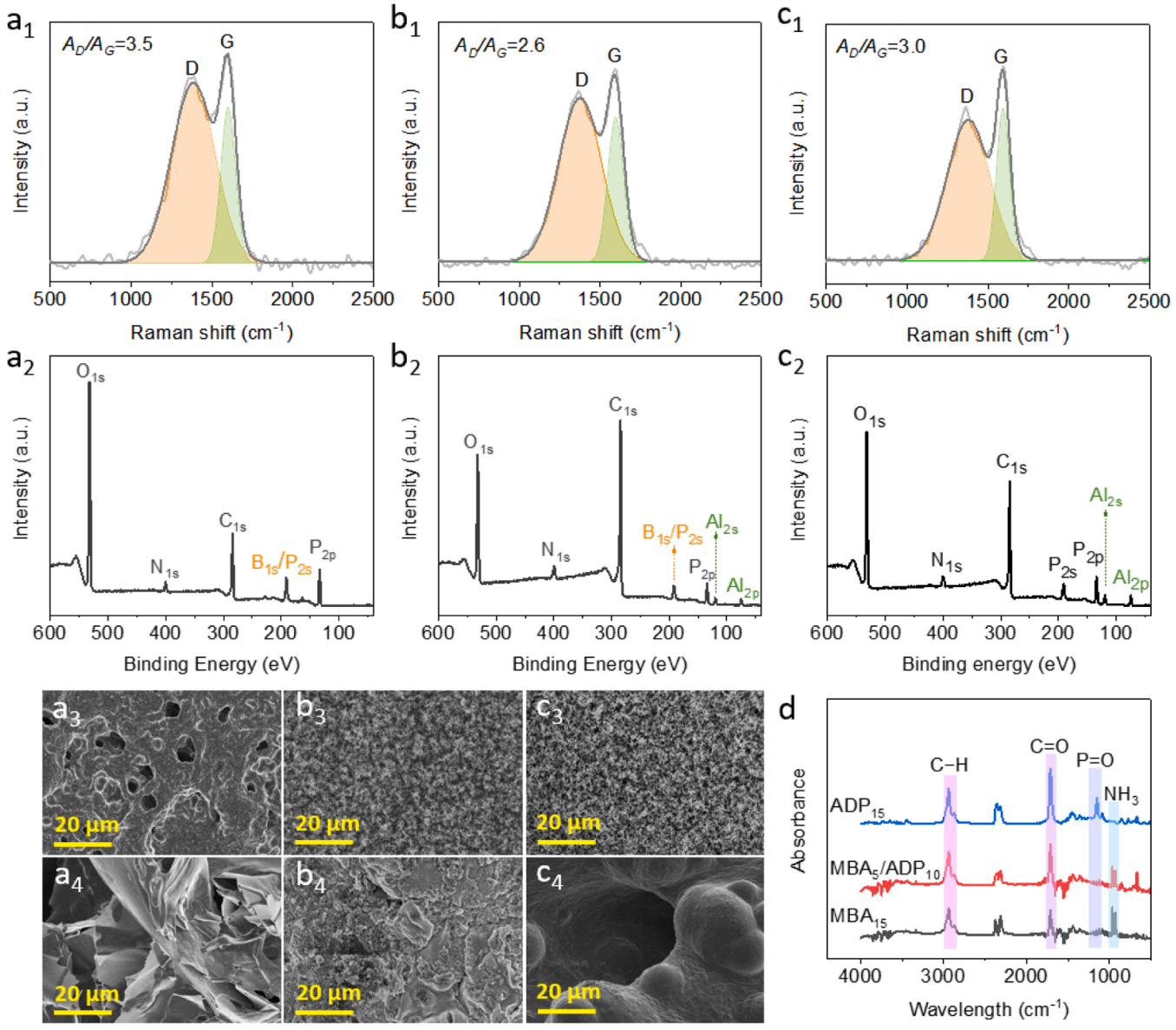

Fig. 7. (a_1-c_1) Raman spectroscopy, (a_2-c_2) XPS spectra, (a_3-c_3) SEM images of external chars /(a_4-c_4) internal chars of char residues of FRPA6; (d) TG-IR spectra at 450 °C of MBA_{15}, MBA_5/ADP_{10}, ADP_{15}.

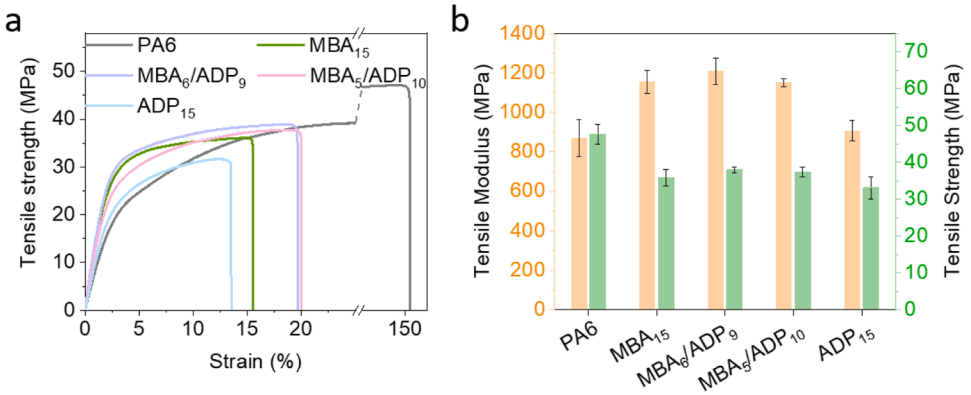

Fig. 8. (a) Typical stress-stain curves and (b) tensile strength & tensile modulus of PA6 and its fire-retardant systems.

than those of MBA_{15} and MBA_5/ADP_{10} indicate more free radicals released into the gas phase, and thus the residue of ADP_{15} contains less related components, confirming its poor charring ability. MBA_{15} and MBA_5/ADP_{10} release a lot of incombustible N-containing gases (sharp peaks at 930 and 970 cm^{-1}) [49]. Consequently, the inclusion of MBA enhances the gas-phase fire retardancy of PA6/ADP composite.

3.5. Mechanical performances

The mechanical properties, including tensile strength, elongation at break and tensile modulus, of PA6 and FRPA6 were also studied (Fig. 8 and Table S3). Neat PA6 exhibits excellent mechanical performances, such as a tensile strength of ~ 47 MPa, an elongation at break of ~ 150% and a tensile modulus of ~ 847 MPa [49]. The fracture cross-section of PA6 looks rather rough, and many vacancies can be observed with a certain orientation due to the deformation of PA6 chains in the tension direction, indicative of a ductile fracture mode (Fig. S2a). The addition of fire retardants induces substantial reductions in both tensile strength and elongation at break to 33 ~ 36 MPa and 14 % ~ 19 %, but an increased elastic modulus to 1206 MPa. In comparison with ADP, MBA can better preserve the mechanical strength of PA6. For instance, The MBA_6/ADP_9 sample possesses the best mechanical properties among all FRPA6 composites (tensile strength: ~38 MPa, tensile modulus: ~1206 MPa, and elongation at break: ~19 %), followed by MBA_5/ADP_{10}. This can be reflected by their SEM images. For instance, the MBA_5/ADP_{10} shows a rough fracture surface with many wrinkles due to the polymer matrix deformation (Fig. S2b). In comparison, the ADP granules (Fig. S2e) scattered in the PA6 matrix severely restrict the deformability of the polymer matrix, leading to a nearly brittle fracture mode without any matrix deformation traces (Fig. S2c). The EDS mapping (Fig. S2d) of MBA_5/ADP_{10} also shows that MBA and ADP are evenly dispersed within the PA6 matrix. As a consequence, the synergistic MBA/ADP system endows PA6 with better mechanical strength and rigidity than PA6/ADP composites.

4. Conclusion

In this study, a P/N/B-containing aggregate (MBA) has been synthesized via a green strategy by using water as the solvent. MBA is then employed as a synergist for fire-retardant PA6/ADP composites. Regardless of its poor fire-retardancy efficiency, MBA possesses a strong carbonization ability. The use of MBA to replace an equal loading level of ADP can significantly improve the fire performance of PA6 with significantly decreased heat release and increased residue yields, apart from the well-retained UL-94 V-0 rating and increased LOI. Specifically, the incorporation of 5 wt% MBA and 10 wt% ADP brings about 52.5 %, 18.6%, 15.3 % and 36.2 % reductions in PHRR, THR, AEHC and MARHE compared to neat PA6 in the cone test, respectively, while only 21.5 %, 9.6 %, 10.5 % and minus reductions in them are achieved by ADP_{15}. Besides, this combination formula leads to the highest FRI value (1.84), implying a better fire retardancy. Furthermore, MBA shows an ability to boost the fire retardancy of PA6/ADP composite via synergy, as reflected by a high synergisitc effectivity of 55.4 % in terms of PHRR reduction, and a more significant heat inhibition effect during combustion. Regarding the mode of action, the MBA and ADP combination performs the flame inhibition in the gas phase and plays a barrier-protective role in the condensed phases. Besides, MBA and ADP also shows a synergy in improving mechanical properties of PA6. This work provides a multi-element and synergistic strategy for improving the fire safety of PA6, and is expected to significantly expand the application of PA6 in the indsutry.

CRediT authorship contribution statement

Yixia Lu: Writing – original draft, Methodology, Investigation, Data curation, Conceptualization. **Tao Chu:** Investigation, Data curation. **Siqi Huo:** Writing – review & editing. **Guobo Huang:** Writing – review & editing. **Zhiguang Xu:** Writing – review & editing, Supervision, Project administration. **Jiabing Feng:** Writing – review & editing, Supervision, Methodology. **Hongyan Xie:** Writing – review & editing, Formal analysis. **Pooya Jafari:** Methodology, Formal analysis. **Hao Wang:** Writing – review & editing. **Pingan Song:** Writing – review & editing, Supervision, Conceptualization.

Declaration of competing interest

The authors declare that they have no known competing financial interests or personal relationships that could have appeared to influence.

Data availability

No data was used for the research described in the article.

Acknowledgments

This work was financially supported by the Australian Research Council(Grant No. LP220100278, DP240102628, DP240102728), and the Project for Science and Technology Innovation Leading Talents of Zhejiang Provincial High-level Talents Special Support Plan (Grant No. 2021R52028).

Supplementary materials

Supplementary material associated with this article can be found, in the online version, at doi:10.1016/j.polymdegradstab.2024.110949.

References

[1] S. Fan, B. Peng, R. Yuan, D. Wu, X. Wang, J. Yu, F. Li, A novel Schiff base-containing branched polysiloxane as a self-crosslinking flame retardant for PA6 with low heat release and excellent anti-dripping performance, Compos. B. Eng. 183 (2020) 107684–107694, https://doi.org/10.1016/j.compositesb.2019.107684.

[2] Y. Li, J. Wang, B. Xue, S. Wang, P. Qi, J. Sun, H. Li, X. Gu, S. Zhang, Enhancing the flame retardancy and UV resistance of polyamide 6 by introducing ternary supramolecular aggregates, Chemosphere 287 (Pt 2) (2022) 132100–132109, https://doi.org/10.1016/j.chemosphere.2021.132100.

[3] M. Qian, Y. Sun, X. Xu, L. Liu, P. Song, Y. Yu, H. Wang, J. Qian, 2D-alumina platelets enhance mechanical and abrasion properties of PA612 via interfacial hydrogen-bond interactions, Chem. Eng. J. 308 (2017) 760–771, https://doi.org/10.1016/j.cej.2016.09.124.

[4] P. Song, C. Wang, L. Chen, Y. Zheng, L. Liu, Q. Wu, G. Huang, Y. Yu, H. Wang, Thermally stable, conductive and flame-retardant nylon 612 composites created by adding two-dimensional alumina platelets, Compos. Part A Appl. Sci. Manuf. 97 (2017) 100–110, https://doi.org/10.1016/j.compositesa.2017.02.029.

[5] Y. Lu, J. Feng, D. Yi, H. Xie, Z. Xu, C.F. Cao, S. Huo, H. Wang, P. Song, Strong synergistic effects between P/N-containing supramolecular microplates and aluminum diethylphosphinate for fire-retardant PA6, Compos. Part A Appl. Sci. Manuf. 176 (2024) 107834–107843, https://doi.org/10.1016/j.compositesa.2023.107834.

[6] H. Feng, Y. Qiu, L. Qian, Y. Chen, B. Xu, F. Xin, Flame inhibition and charring effect of aromatic polyimide and aluminum diethylphosphinate in polyamide 6, Polymers (Basel) 11 (1) (2019) 1–13, https://doi.org/10.3390/polym11010074.

[7] W. He, J. Gao, S. Liao, X. Wang, S. Qin, P. Song, A facile method to improve thermal stability and flame retardancy of polyamide 6, Compos. Commun. 13 (2019) 143–150, https://doi.org/10.1016/j.coco.2019.04.010.

[8] A.D. Naik, G. Fontaine, F. Samyn, X. Delva, Y. Bourgeois, S. Bourbigot, Melamine integrated metal phosphates as non-halogenated flame retardants: synergism with aluminium phosphinate for flame retardancy in glass fiber reinforced polyamide 66, Polym. Degrad. Stab. 98 (12) (2013) 2653–2662, https://doi.org/10.1016/j.polymdegradstab.2013.09.029.

[9] S. Huo, S. Yang, J. Wang, J. Cheng, Q. Zhang, Y. Hu, G. Ding, Q. Zhang, P. Song, A liquid phosphorus-containing imidazole derivative as flame-retardant curing agent for epoxy resin with enhanced thermal latency, mechanical, and flame-retardant performances, J. Hazard. Mater. 386 (2020) 121984–121993, https://doi.org/10.1016/j.jhazmat.2019.121984.

[10] J. Feng, Z. Ma, Z. Xu, H. Xie, Y. Lu, C. Maluk, P. Song, S. Bourbigot, H. Wang, A Si-containing polyphosphoramide via green chemistry for fire-retardant polylactide with well-preserved mechanical and transparent properties, Chem. Eng. J. 431 (2022) 134259–134271, https://doi.org/10.1016/j.cej.2021.134259.

[11] J. Feng, Y. Lu, H. Xie, Y. Zhang, S. Huo, X. Liu, M. Flynn, Z. Xu, P. Burey, M. Lynch, et al., Atom-economic synthesis of an oligomeric P/N-containing fire retardant towards fire-retarding and mechanically robust polylactide biocomposites, J. Mater Sci. Technol. 160 (2023) 86–95, https://doi.org/10.1016/j.jmst.2023.04.003.
[12] T. Rahimi-Aghdam, Z. Shariatinia, M. Hakkarainen, Haddadi-Asl, V. Nitrogen and phosphorous doped graphene quantum dots: excellent flame retardants and smoke suppressants for polyacrylonitrile nanocomposites, J. Hazard. Mater. 381 (2020) 121013–121028, https://doi.org/10.1016/j.jhazmat.2019.121013.
[13] P. Li, C. Liu, Y.-J. Xu, Z.-M. Jiang, Y. Liu, P. Zhu, Novel and eco-friendly flame-retardant cotton fabrics with lignosulfonate and chitosan through LbL: flame retardancy, smoke suppression and flame-retardant mechanism, Polym. Degrad. Stab. 181 (2020) 109302–109312, https://doi.org/10.1016/j.polymdegradstab.2020.109302.
[14] S. Fan, C. Zhu, D. Wu, X. Wang, J. Yu, F. Li, Silicon-containing inherent flame-retardant polyamide 6 with anti-dripping via introducing ethylene glycol as the chain-linker and charring agent, Polym. Degrad. Stab. 173 (2020) 109080–109090, https://doi.org/10.1016/j.polymdegradstab.2020.109080.
[15] Z. Wang, W. Wu, Z. Liu, H. Shen, Y. Feng, Study on novel boron-containing triazine flame retarded thermoplastic polyester elastomer composites and the flame retardant mechanism, React. Funct. Polym. 190 (2023) 105621–105630, https://doi.org/10.1016/j.reactfunctpolym.2023.105621.
[16] C. Ling, L. Guo, Recent developments and applications of hyperbranched polymers as flame retardants, J. Anal. Appl. Pyrolysis 169 (2023) 105842–105852, https://doi.org/10.1016/j.jaap.2022.105842.
[17] J. Green, Mechanisms for flame retardancy and smoke suppression -a review, J. Fire Sci. 14 (6) (1996) 426–442, https://doi.org/10.1177/073490419601400602.
[18] R.K. Jian, X.B. Lin, Z.Q. Liu, W. Zhang, J. Zhang, L. Zhang, Z. Li, D.Y Wang, Rationally designed zinc borate@ZIF-8 core-shell nanorods for curing epoxy resins along with low flammability and high mechanical property, Compos. B. Eng. 200 (2020) 108349–108358, https://doi.org/10.1016/j.compositesb.2020.108349.
[19] Z. Ma, J. Zhang, C. Maluk, Y. Yu, S.M. Seraji, B. Yu, H. Wang, P. Song, A lava-inspired micro/nano-structured ceramifiable organic-inorganic hybrid fire-extinguishing coating, Matter 5 (3) (2022) 911–932, https://doi.org/10.1016/j.matt.2021.12.009.
[20] Z. Wang, T. Zhang, M. Hao, M. Li, Y. Zhou, W. Sun, J. Wang, Y. Cheng, Novel multifunctional melamine borate - boron nitride nanosheets/epoxy composites with enhanced thermal conductivity, flame retardancy and satisfying electrical insulation, Compos. Part A Appl. Sci. Manuf. 169 (2023) 107495–107509, https://doi.org/10.1016/j.compositesa.2023.107495.
[21] P. Khalili, X. Liu, K.Y. Tshai, et al., Development of fire retardancy of natural fiber composite encouraged by a synergy between zinc borate and ammonium polyphosphate, Compos. Part B Eng. 159 (2019) 165–172, https://doi.org/10.1016/j. compositesb.2018.09.036.
[22] M. Dogan, S.D. Dogan, L.A. Savas, G. Ozcelik, U. Tayfun, Flame retardant effect of boron compounds in polymeric materials, Compos. B. Eng. 222 (2021) 109088–109115, https://doi.org/10.1016/j.compositesb.2021.109088.
[23] B.P. Mishra, P. Babu, K. Parida, Phosphorous, boron and sulfur doped g-C3N4 nanosheet: synthesis, characterization, and comparative study towards photocatalytic hydrogen generation, Mater. Today: Proc. 35 (2021) 258–262, https://doi.org/10.1016/j.matpr.2020.05.567.
[24] J. Liu, P. Qi, D. Meng, L. Li, J. Sun, H. Li, X. Gu, S. Jiang, S. Zhang, Eco-friendly flame retardant and smoke suppression coating containing boron compounds and phytic acids for nylon/cotton blend fabrics, Ind. Crops. Prod. 186 (2022), https://doi.org/10.1016/j.indcrop.2022.115239.
[25] M. Doğan, E. Bayramlı, Effect of boron-containing materials on the flammability and thermal degradation of polyamide 6 composites containing melamine, J. Appl. Polym. Sci. 118 (5) (2010) 2722–2727, https://doi.org/10.1002/app.32637.
[26] Y. Yi, J. Wang, Y. Niu, Y. Yu, S. Wu, K. Ding, Exploring the evolution patterns of melem from thermal synthesis of melamine to graphitic carbon nitride, RSC Adv. 12 (37) (2022) 24311–24318, https://doi.org/10.1039/d2ra03337b.
[27] X. Yuan, K. Luo, Y. Wu, J. He, Z. Zhao, D. Yu, Investigation on the stability of derivative melam from melamine pyrolysis under high pressure, Nanomaterials (Basel) 8 (3) (2018) 172–179, https://doi.org/10.3390/nano8030172.
[28] J. Lazko, N. Landercy, F. Laoutid, L. Dangreau, M.H. Huguet, O. Talon, Flame retardant treatments of insulating agro-materials from flax short fibres, Polym. Degrad. Stab. 98 (5) (2013) 1043–1051, https://doi.org/10.1016/j.polymdegradstab.2013.02.002.
[29] S. Huo, T. Sai, S. Ran, Z. Guo, Z. Fang, P. Song, H. Wang, A hyperbranched P/N/B-containing oligomer as multifunctional flame retardant for epoxy resins, Compos. B. Eng. 234 (2022) 109701–109712, https://doi.org/10.1016/j.compositesb.2022.109701.
[30] W. He, H. Xu, P. Song, Y. Xiang, S.P. Qin, N-decorated halloysite nanotubes for flame retardancy enhancement of polyamide 6/aluminum diethylphosphinate, Polym. Degrad. Stab. 196 (2022), https://doi.org/10.1016/j.polymdegradstab.2022.109847, 109847-100857.
[31] H. Vothi, C. Nguyen, L.H. Pham, J. Kim, D. Hoang, Degradation mechanism and flame retardancy of aluminum phosphonate in glass fiber-reinforced poly(butylene terephthalate), Polym. Bull. 78 (12) (2021) 6761–6776, https://doi.org/10.1007/s00289-020-03455-2.
[32] F. Samyn, S. Bourbigot, Thermal decomposition of flame retarded formulations PA6/aluminum phosphinate/melamine polyphosphate/organomodified clay: interactions between the constituents? Polym. Degrad. Stab. 97 (11) (2012) 2217–2230, https://doi.org/10.1016/j.polymdegradstab.2012.08.004.
[33] A. Wirasaputra, L. Zheng, S. Liu, Y. Yuan, J. Zhao, High-performance flame-retarded polyamide-6 composite fabricated by chain extension, Macromol Mater Eng 301 (5) (2016) 614–624, https://doi.org/10.1002/mame.201500357.
[34] T. Liang, J. Cai, S. Liu, H. Lai, J. Zhao, Chain extension and synergistic flame-retardant effect of aromatic schiff base diepoxide on polyamide 6/aluminum diethylphosphinate composites, Materials (Basel) 12 (14) (2019) 2217–2233, https://doi.org/10.3390/ma12142217.
[35] J. Li, L. Qian, W. Xi, J. Wang, Y. Qiu, Y. Chen, W. Tang, Alloying synergistic flame retardant effect on PA6 by polyimide containing alkyl hypophosphate structure, Eur. Polym. J. 211 (2024) 113033–113045, https://doi.org/10.1016/j.eurpolymj.2024.113033.
[36] B. Schartel, T.R. Hull, Development of fire-retarded materials—interpretation of cone calorimeter data, Fire Mater 31 (5) (2007) 327–354, https://doi.org/10.1002/fam.949.
[37] L. Liu, M. Zhu, Z. Ma, X. Xu, S. Mohesen Seraji, B. Yu, Z. Sun, H. Wang, P. Song, A reactive copper-organophosphate-MXene heterostructure enabled antibacterial, self-extinguishing and mechanically robust polymer nanocomposites, Chem. Eng. J. 430 (2022) 132712–132723, https://doi.org/10.1016/j.cej.2021.132712.
[38] H. Vahabi, B.K. Kandola, M.R. Saeb, Flame retardancy index for thermoplastic composites, Polymers (Basel) 11 (3) (2019) 407–416, https://doi.org/10.3390/polym11030407.
[39] P. Wiśniewska, E. Movahedifar, K. Formela, M.Z. Naser, H. Vahabi, M.R. Saeb, The chemistry, properties and performance of flame-retardant rubber composites: collecting, analyzing, categorizing, machine learning modeling, and visualizing, Compos. Sci. Technol. 250 (2024), https://doi.org/10.1016/j.compscitech.2024.110517.
[40] M. Lewin, Synergism and catalysis in flame retardancy of polymers, Polym. Adv. Technol. (12) (2001) 215–222, https://doi.org/10.1002/pat.132.
[41] H. Lu, C.A. Wilkie, Synergistic effect of carbon nanotubes and decabromodiphenyl oxide/Sb2O3 in improving the flame retardancy of polystyrene, Polym. Degrad. Stab. 95 (4) (2010) 564–571, https://doi.org/10.1016/j.polymdegradstab.2009.12.011.
[42] S. Brehme, B. Schartel, J. Goebbels, O. Fischer, D. Pospiech, Y. Bykov, M. Döring, Phosphorus polyester versus aluminium phosphinate in poly(butylene terephthalate) (PBT): flame retardancy performance and mechanisms, Polym. Degrad. Stab. 96 (5) (2011) 875–884, https://doi.org/10.1016/j.polymdegradstab.2011.01.035.
[43] J. Wang, L. Qian, Z. Huang, Y. Fang, Y. Qiu, Synergistic flame-retardant behavior and mechanisms of aluminum poly-hexamethylenephosphinate and phosphaphenanthrene in epoxy resin, Polym. Degrad. Stab. 130 (2016) 173–181, https://doi.org/10.1016/j.polymdegradstab.2016.06.010.
[44] J. Zhang, A. Koubaa, D. Xing, W. Liu, Q. Wang, X. Wang, H. Wang, Improving lignocellulose thermal stability by chemical modification with boric acid for incorporating into polyamide, Mater. Des. 191 (2020) 108589, https://doi.org/10.1016/j.matdes.2020.108589.
[45] W.X. Li, H.J. Zhang, X.P. Hu, W.X. Yang, Z. Cheng, C.Q. Xie, Highly efficient replacement of traditional intumescent flame retardants in polypropylene by manganese ions doped melamine phytate nanosheets, J. Hazard. Mater. 398 (2020) 123001–123013, https://doi.org/10.1016/j.jhazmat.2020.123001.
[46] J. Feng, Y. Lu, H. Xie, Z. Xu, G. Huang, C.F. Cao, Y. Zhang, V.S. Chevali, P. Song, H. Wang, Solvent-free synthesis of organic–inorganic polyphosphoramide-halloysite nanohybrids for thermally stable and fire-resistant polylactide, ACS Sustain. Chem. Eng. 10 (46) (2022) 15223–15232, https://doi.org/10.1021/acssuschemeng.2c04899.
[47] J.W. Hastie, Molecular basis of flame inhibition, J. Res. Natl. Bur. Stand. A. Phys. Chem. 77A (1973) 733–754, https://doi.org/10.6028/jres.077A.045.
[48] J. Feng, X. Xu, Z. Xu, H. Xie, P. Song, L. Li, G. Huang, H. Wang, One-pot, solvent- and catalyst-free synthesis of polyphosphoramide as an eco-benign and effective flame retardant for poly(lactic acid), ACS Sustain. Chem. Eng. 8 (44) (2020) 16612–16623, https://doi.org/10.1021/acssuschemeng.0c05931.
[49] Y. Lu, J. Feng, T. Chu, S. Huo, H. Xie, Z. Xu, H. Wang, P. Song, A 2D biobased P/N-containing aggregate for boosting fire retardancy of PA6/aluminum diethylphosphinate via synergy, J. Mater Sci. Technol. 198 (2024) 73–82, https://doi.org/10.1016/j.jmst.2024.03.001.